Electronic states in semiconductor double quantum dots and quantum rings - Theory and tight-binding modeling

Calle J. Stenberg

June 10, 2021

A Master Thesis at the
Division of Solid State Physics

Lund University

Supervisors

Martin Leijnse
Athanasios Tsintzis

Contents

Abstract

In recent experiments on semiconductor nanowires and quantum dots, enhanced g-factors up to several times the bulk value have been measured [1] [2]. The enhancement is attributed to orbital contributions g^*_{orb} to the effective g-factor $g^* = g^*_{spin} + g^*_{orb}$ from the coupling of the high angular momentum ring-like states to the magnetic field. The objective of the work presented here is to model the double quantum dot (DQD) system in [1], extending previous theoretical models to a two-dimensional (2D) tight-binding ring-shaped structure using the open-source python package Kwant [3]. It is found that the enhanced g-factors can be straightforwardly predicted by the model because of the formation of ring-like states when an even orbital on one dot aligns with an odd orbital in the other dot. Ring states require combinations of even and odd orbitals at zero magnetic field, even-even (similarly odd-odd) orbital parity combinations lead to poor ring formation. Moreover, Aharonov-Bohm oscillations are also present in the model when the ring is penetrated by a significant flux in agreement with recent experimental findings in similar systems. The states of interest transforms from crossing to anti-crossing when increasing the flux through the ring from 0 to $\frac{1}{2}$ flux quanta as the parity requirement of the aligned orbitals to form ring states are reversed. This means at $\frac{1}{2}$ flux quanta the condition of even-odd orbital alignment to form good ring states is broken and even-even and odd-odd orbital combinations form good ring states instead. The model presented here is a more realistic description of the real experimental system compared with previous theory and the results are consistent with experimental findings.

1 Introduction

Semiconductor technology has undoubtedly revolutionized electronics and shaped the society. From the invention of the first operational transistor at Bell Labs in 1947 the number of transistors on a given circuit has grown exponentially far greater than anticipated. The A14 processor is commercially offering node sizes of 5 nm in Apple products and plans for the 3 nm node exist [4]. Transistor conductivity is controlled by an electric potential applied via a capacitively coupled gate. The gate is separated from the structure by an insulating oxide. Due to quantum tunneling through the gate oxide causing a leakage of carriers, device conductivity on these small scales are becoming increasingly difficult to mange. At some point the current semiconductor technologies require a transition to a drastically new type of technology.

One possible drastic change would be quantum information processing. Quantum information is an emerging field with possibilities to revolutionize modern computation and communication. The fundamental unit of information in quantum computation is the quantum mechanical correspondence of a bit, the qubit. Information is no longer binary but consists of entangled quantum states. States can be manipulated by quantum gates and are anticipated to lead to more complex and effective computations compared to traditional transistor technologies [5].

The importance of quantum effects is not limited to quantum information processing devices. In general, as device dimensions approach the wavelength of electrons and holes, quantum properties play a major role. In bulk materials the electrons are free to move in all directions and as a result, continuous energy bands are formed. As a dimension is reduced the electron experiences confinement and quantized motion in that direction. A visualization of confinement in 1,2 and 3 dimensions can be seen in Fig 1. The quantization of motion directly influences the energy spectrum and in 3D confinement (0D material) the electron energy levels are discrete. Such a

system is commonly known as a quantum dot.

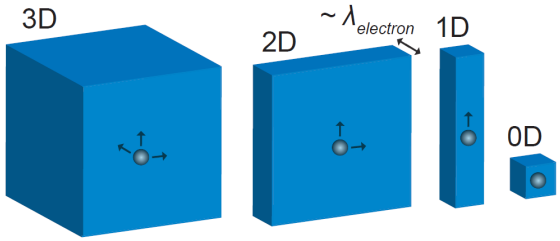

Figure 1: Motion of electrons in materials of different dimensions. Figure taken from [6].

The quantization of energy, orbital and spin degrees of freedom of the quantum dot resemble the atom. The ability to manipulate these properties makes the quantum dot excellent for studying fundamental physics and highly interesting in electronics and is already applied in numerous components. Quantum dots are for example used in medicine as tunable dye, in improving light sources such as LEDs and LASERs [7] and in the realization of true RGB pixels in displays [8].

One of the most exciting applications is the realization of the so called spin qubit which is promising as the main building block in quantum computation [9]. Quantum dots (QDs) are of high interest in the realization of spin-based qubits due to the discrete energy levels and the ability to control spin dynamics. One way to manipulate quantum spin states utilizes spin-orbit coupling (SOC). This requires strong spin-orbit interaction where the electron orbital motion couples strongly to the electron spin. By the use of electric fields the spin states can be efficiently controlled to store and manipulate information for quantum computing [10].

There are a number of ways to realize quantum dots, this thesis will focus on quantum dots epitaxially defined in nanowires [6]. Nanowires are quasi-1D structures where electrons are confined in two dimensions but are free to more longitudinally, see Fig. 1. Due to advances in material science the growth of nanowires can be controlled up to single atomic layer precision and relaxation of crystal lattice matching in nanowires enables interesting combinations of III-V semiconductors of different crystal structures such as Wurtzite and Zinc blende InAs to define a quantum dot [11] [12]. By defining closely separated regions of high bandgap material a quantum well is formed [13], visualized in Fig. 2. Since the well is confined in three dimensions it behaves as a quasi zero-dimensional quantum dot.

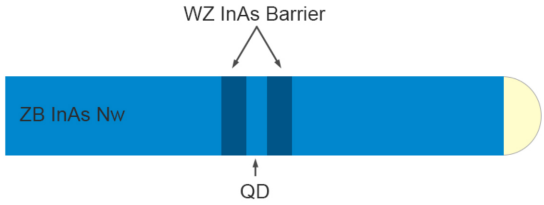

Figure 2: Schematic representation of a Zinc Blende InAs nanowire defined quantum dot confined between thin segments of Wurtzite InAs.

Two potential pockets can spontaneously form within the QD in Fig.2 due to surface charges of the nanowire and to tuning connected side gates (not visualised yet). The two pockets acts as two parallel-coupled dots. This is the double quantum dot system of interest, see Fig 3 [6].

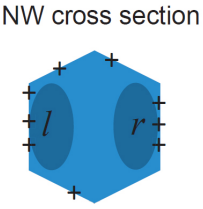

Figure 3: Schematic representation of potential pockets formation (darker region) due to uneven surface charge distribution and thus the realisation of a DQD system. Figure taken from [6].

1.1 Quantum Ring Theory

In recent works it has been observed how the effective g-factor of semiconductor nanowires experiences an enhancement up to several times of the bulk value [1], in contrast to the expectation

that confinement would reduce the effective g-factor [2]. The most common way to rotate spin states is by an oscillating magnetic field [14]. The efficiency to which this is achieved depends on the g-factor. Having large g-factors are therefore desirable as it allows spin rotation using smaller magnetic fields. Moreover, as will become more clear later the g-factor in this particular system can be tuned dramatically using electric fields. A possible way to achieve spin rotation is then to have a constant magnetic field and tune the g-factor using an electric field. Manipulation of electric fields are generally significantly more effective than manipulation of magnetic fields and this way of inducing spin rotations are a rare property and possibly very valuable. The appearance of enhanced g-factors is explained by strong orbital effects of higher subbands and the formation of quantum rings. In [2] the quantum rings form due to rotational symmetric nanowires whereas in [1] the ring states form despite the lack of rotational symmetry. By manipulation of magnetic and electric fields the formation of quantum rings is possible, even in a non rotationally symmetric system. In this thesis the experimentally observed effect on the effective g-factor of these formations will be modeled using an extension of the 1D model in [1] to a 2D tight-binding model.

To illustrate the meaning of quantum rings the 1D ring wave function can be determined, starting from the free particle Schrödinger equation

$$-\frac{\hbar^2}{2m_e}\nabla^2\psi = E\psi. \tag{1}$$

For a cylindrical system Eq. 1 can be represented in polar coordinates

$$-\frac{\hbar^2}{2m_eR^2}\frac{\partial^2}{\partial\theta^2}\psi = E\psi, \tag{2}$$

where R is the ring radius and θ the angular coordinate. The solutions to this differential equation are

$$\psi_m(\theta) = \frac{1}{\sqrt{2\pi}}e^{im\theta}, E_m = \frac{\hbar^2m^2}{2m_eR^2} \tag{3}$$

where $m = 0, \pm1, \pm2, \pm3...$ as the boundary condition of a ring requires $e^{im(\theta+2\pi)=e^{im\theta}}$. These are the quantum ring states. The angular momentum of the ring states is given by $\hat{L}_z|m\rangle = m\hbar|m\rangle$.

It was found in [1] that in a specific gate potential configuration, double quantum dot (DQD) systems where the dots are coupled in two points also exhibit ring-like states, surprisingly. The specifics of the system modeled will be presented in Section 2. It was found that despite the significant tunnel barriers between the double quantum dots quantum ring states form, if two criteria are fulfilled. The tunneling coupling strength at the connection points between the two quantum dots have to be identical and the aligned energy levels of the two quantum dots have to be combinations of even and odd orbitals [1].

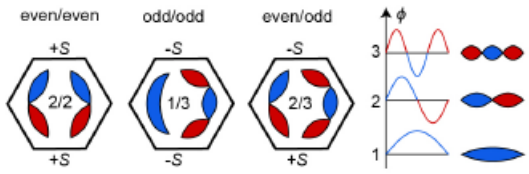

Figure 4: Schematic representation of different aligned orbitals in the double quantum dot. The ring states can only be observed in the even/odd orbital combination. Figure taken from [1].

Each electron pocket in Fig. 3 can be thought of as two adjacent particle in a box system. The electrons in a particle in a box picture have discrete energy levels of different symmetry. The first 3 modes in such a system is visualized to the right in Fig. 4. What is meant by aligning combinations of even and odd orbitals is adjusting the gate potential in such a way that one well has an even mode aligned with an odd mode in the other well. In the case of even and odd orbital alignment visualized in Fig. 4, the hybridization energy vanishes due to different signs in the overlap integral and results in the formation of two ideal ring states. In the ring-like hybridized wave function the electrons are free to orbit clockwise or anti-clockwise. Calculating the expectation

value of the angular momentum operator yields a quantitative indication of ring state quality. This property will be used in evaluating the ring states.

Moreover, due to the Aharonov-Bohm effect covered in section 1.1.1, if magnetic flux equal to $\frac{1}{2}\ h/e$ is fed through the ring, the overlap integral receives an additional minus sign in one of the tunnel couplings [1]. This results in even-even and odd-odd symmetry orbitals having vanishing hybridization energies and thus becoming ring states, while the even-odd orbitals become poor ring states.

A special feature of ring states in magnetic fields is that the effective g-factor is given by a sum of spin (Zeeman) and orbital contributions $g^* = g^*_{spin} + g^*_{orb}$. The g-factor is a dimensionless proportionality constant and characterizes how the electron spin couples to an external magnetic field. Due to the orbital effects in finite angular momentum quantum ring states g^* experiences enhancement. This will be discussed in more detail in Section 1.2. The ability to control the quality of ring states by manipulating the electric field and thus the orbital alignments, leads to the possibility of tuning the orbital contributions to the effective g-factor over large ranges. In this thesis it will be confirmed that the magnetic flux influence on the orbital contributions of quantum ring states indeed explains the appearance of g-factor enhancement in a nanowire DQD and can be straightforwardly predicted using a 2D tight-binding model.

1.1.1 Aharonov-Bohm Effect

A fundamental feature of ring states is the appearence of the Aharonov-Bohm (AB) effect as mentioned briefly in the previous section. In 1959 Y. Yakir Aharonov and David Bohm proved that electrons can be affected by the magnetic vector potential $\mathbf{A}$ in regions of space where the magnetic field $\mathbf{B}$ is zero [15]. For more insight and detailed derivations see [16].

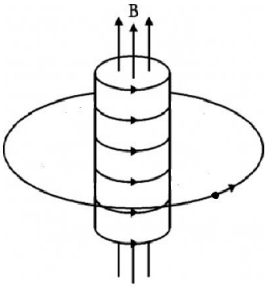

Figure 5: Illustration of a charged particle travelling around a solenoid with a magnetic field inside. The particle is not directly influenced by the magnetic field but due to the AB effect the effect of the vector potential cannot be excluded. Figure taken from [16].

If a charged particle travels in a closed loop around a conducting solenoid with a magnetic field inside, no field is directly acting upon the particle, see Fig. 5. However, due to the vector potential of the magnetic field the particle energy is still affected. The root of this effect stems from the quantum mechanical formalism where eliminating the vector potential is not possible. This is in contrast with classical mechanics where the equation of motion is expressed in the field alone and the vector potential is regarded as a mathematical tool and not a real physical observable.

Now consider the free particle Hamiltonian

$$H = \frac{\hat{p}^2}{2m_e}, \hat{p} = -i\hbar\nabla. \tag{4}$$

In the presence of a magnetic field the momentum is replaced by the kinetic momentum

$$H = \frac{(\hat{p} - e\mathbf{A})^2}{2m_e}, \tag{5}$$

including the magnetic vector potantial $\mathbf{A}$. Expanding the square, setting $e = 1$ and explicitly writing $\hat{p} = -i\hbar\nabla$, results in

$$H = \frac{\hat{p}^2 + (\hat{p}\mathbf{A} + \mathbf{A}\hat{p}) + \mathbf{A}^2}{2m_e}, \tag{6}$$

$$= -\frac{\hbar^2}{2m_e}\nabla^2 - \frac{i\hbar}{2m_e}(\nabla\mathbf{A} + \mathbf{A}\nabla) + \frac{\mathbf{A}^2}{2m_e}. \tag{7}$$

The vector potential $\mathbf{A}$ can be chosen to have zero divergence (Coulomb gauge)

$$\nabla \cdot \mathbf{A} = 0. \tag{8}$$

In this gauge the nabla operator ∇ and $\mathbf{A}$ commute,

$$\nabla\mathbf{A} + \mathbf{A}\nabla = 2\mathbf{A}\nabla, \tag{9}$$

leading to the Hamiltonian of a free electron in the presence of an magnetic field

$$H = -\frac{\hbar^2}{2m_e}\nabla^2 - \frac{i\hbar}{m_e}(\mathbf{A}\nabla) + \frac{\mathbf{A}^2}{2m_e}. \tag{10}$$

The fact that the vector potential cannot be eliminated results in electrons being influenced by the potential even if no magnetic field acts upon them.

Calculating the state energies for the ideal 1D ring states in Eq. (3) in the above Hamiltonian yields

$$E_m = \frac{1}{m_e}(\frac{\hbar^2 m^2}{2R^2} + \frac{\hbar m A_\theta}{R} + \frac{\mathbf{A}^2}{2}) \tag{11}$$

where A_θ is the vector component along θ. Comparing E_m in Eq. (11) to Eq. (3) reveals additional terms stemming from the inclusion of the vector potential. The first term in Eq. (11) is the same as the free particle energy in Eq. (3). The second term reveals that the electron energy either increase or decrease depending on the sign of m. This means that right moving electrons couple differently to the vector potential than left moving electrons. The state energy no longer depends solely on m but also on the magnitude of the vector potential in both the second and third term.

Moving over to a short introduction of AB oscillations which will be useful later to understand recent unpublished experimental result and their appearance in the model. Electrons enclosing a magnetic flux experience a phase shift dependent on the vector potential $\mathbf{A}$ [15]. Electrons encircling in opposing directions pick up different phases. This results in a cycling of constructive and destructive interference with a period of $\Phi_0 = h/e$ referred to as the magnetic flux quantum [17]. The magnetic flux is defined as the surface integral of the norm to the magnetic field $\mathbf{B}$, as such the flux is both $\mathbf{B}$ and area dependent. The flux quantum can be seen as a flux corresponding to a phase shift to the electron wave function that leaves the electron in the same phase as for zero field, $e^{i\Phi/2} = e^{i(\Phi+2\pi)/2}$. Therefore 1 flux quantum h/e is the required flux for an electron to be phase shifted 1 period 2π in the system.

1.2 Hamiltonian

A semiconductor material (with spin-orbit coupling) is considered in the general case where the $\mathbf{B}$-field is non-zero in the region where the electrons are localized. In the effective mass approximation the Hamiltonian of an electron under the influence of a magnetic field can be expressed as [1] [2]

$$H = H_0 + H_{Zeeman} + H_{SO} + V(r), \tag{12}$$

where H_0 is the free particle Hamiltonian with kinetic momentum given by Eq. (10) , H_{Zeeman} is the Zeeman energy term, H_{SO} the Rashba spin-orbit coupling term and *V(r)* the electrostatic potential.

Introducing both terms separately,

$$H_{Zeeman} = \frac{g^*_{spin}}{2}\mu_B \boldsymbol{\sigma} \cdot \mathbf{B}, \tag{13}$$

$$H_{SO} = \frac{\alpha}{\hbar}(\mathbf{e} \times \mathbf{p}) \cdot \boldsymbol{\sigma}, \tag{14}$$

with g-factor g^*_{spin}, Bohr magneton μ_B , Pauli operator $\boldsymbol{\sigma}$, magnetic field $\mathbf{B}$, Rashba parameter α, electric field direction $\mathbf{e}$ generated by polarization effects in the ZB/WZ junctions and kinetic momentum $\mathbf{p}$.

The Zeeman effect is the splitting of electronic states under the influence of an external magnetic field and is expressed in Eq. (13). The root of the effect is in the spin property of electrons. The degeneracy of electron spin states is disrupted as opposite spins couple differently to

the magnetic field. Eq (13) describe the linear splitting of the states $\Delta E_z = (s_\uparrow - s_\downarrow)|g^*_{spin}|\mu_B \mathbf{B}$, where $s_\uparrow = \frac{1}{2} s_\downarrow = -\frac{1}{2}$. The spin-orbit coupling term in Eq. (14) is a relativistic impact of the electric field on the magnetic moment of the electron and leads to a coupling of orbital motion and spin [18]. In semiconductors it stems from the intrinsic bulk inversion asymmetry of the crystal phase and the extrinsic contribution from the asymmetry in the confining potential [6].
Moreover, in quantum ring states with high orbital angular momentum, results in g^* enhancement up to several times the bulk semiconductor value because of orbital contributions g^*_{orb} to the total g-factor, given by $g^* = g^*_{spin} + g^*_{orb}$.

2 System

In experiments the quantum dot is defined by sandwiching a 5 nm Zinc Blende (ZB) InAs segment between two 25 nm Wurtzite (WZ) InAs segments in a ≈80 nm diameter hexagonal ZB InAs nanowire, as shown in Fig. 2 [1].
The band offsets between WZ and ZB InAs confine carriers in the region and a quantum well is formed. The structure rests upon a global back gate and is capacitively coupled to side gates V_L and V_R, see Fig. 6, allowing for electrostatic control of electron energy levels in the quantum dot.

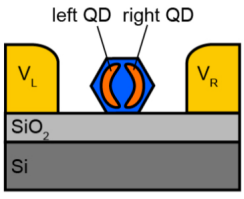

Figure 6: Cross section schematic representation of the double quantum dot states and side gates. Figure taken from [1].

By adjusting applied voltages on the global back gate and side gates V_L and V_R two quantum dots left (L) and right (R) form close to the surface of the quantum dot as visualized in Fig. 6.

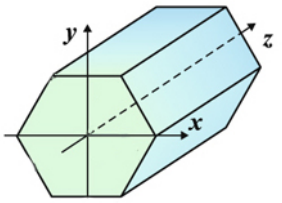

Figure 7: Illustration of the coordinate system of the model with z-direction along the nanowire axis.

Fig. 7 defines the chosen coordinate system in the model. As the depth in z-direction of the quantum dot is ≈ 5 nm and the diameter of the nanowire ≈ 80 nm the electrons are strongly confined in z and the modeled system is approximated as a 2D ring-like structure.

3 Method

As described in the previous section the structure of interest is a double quantum dot epitaxially and electrostatically defined in a hexagonal ZB InAs nanowire. Since the quantum dots are strongly confined in z-direction they are approximated as a 2D circular surface in the xy-plane corresponding to the cross section of the wire. The considered system is circular even though the nanowire is hexagonal. The reason is due to the large nanowire diameter, the electron wave function is mostly localized in the interior of the wire, unaffected by the edges. By adding barriers at the top and bottom of the ring simulates the double quantum dot system visible in Fig. 6 and enforces 2-fold rotational symmetry.

A magnetic field is applied along the z-direction perpendicular to the surface cross section $\mathbf{B} = (0, 0, B_z)$. Choosing the gauge $A_x = A_z = 0$ results in the following vector potential

$$\mathbf{A} = (0, xB_z, 0). \tag{15}$$

Eqs. (10, 13, 14) under the influence of an external magnetic field along the nanowire z-direction and the above gauge can be expressed as

$$H_0 = -\frac{\hbar^2}{2m^*}(\frac{\partial^2}{\partial_x^2} + \frac{\partial^2}{\partial_y^2}) - \frac{ie\hbar}{m^*}xB_z\frac{\partial}{\partial_y} - \frac{e^2x^2B_z^2}{2m^*} \tag{16}$$

$$H_{Zeeman} = \frac{g^*_{spin}\mu_B}{2}\sigma_z \cdot B_z, \tag{17}$$

$$H_{SO} = \alpha(\sigma_x(-i\frac{\partial}{\partial_y} + \frac{exB_z}{\hbar}) + \sigma_y(-i\frac{\partial}{\partial_x})), \tag{18}$$

To arrive at Eq. (18) the electric field **e** in Eq. (14) is chosen along the nanowire z direction.

3.1 Discretization

The tight-binding approximation is achieved by discretizing the continuous position function. The system now consists of sites separated by the lattice constant a. Electrons occupying a site are represented by a discrete position basis state $|x;y>=|ia;ja>=|i;j>$ as the model is two dimensional. The lattice constant a is not necessarily the crystal lattice constant but rather a parameter defining the resolution of the discretization. The first and second order partial derivatives can be expressed as

$$\frac{\partial}{\partial_i} = \frac{1}{2a}\sum |i+1;j\rangle\langle i;j| - |i;j\rangle\langle i+1;j|, \tag{19}$$

$$\frac{\partial^2}{\partial_i^2} = \frac{1}{a^2}\sum |i+1;j\rangle\langle i;j| - 2|i;j\rangle\langle i;j| + |i;j\rangle\langle i+1;j|. \tag{20}$$

By replacing the partials derivaties in Eqs. (16 and 18) with the discretized ones, it is straightforward to calculate the tight-binding matrix elements by mapping the Hamiltonian on the discrete position basis. This yields diagonal and off diagonal elements, more commonly known as onsite and hopping terms. The onsite terms are given by

$$\langle i;j|H|i;j\rangle = (4t + \frac{e^2a^2}{2m^*}B_z^2i^2 + V)\sigma_0 + \frac{\alpha e^2a^2}{\hbar}B_zi\sigma_x + \frac{g^*_{spin}\mu_B}{2}B_z\sigma_z, \tag{21}$$

where σ_0 is a 2x2 identity matrix. The hopping terms are given by

$$\langle i+1;j|H|i;j\rangle = -t\sigma_0 - i\frac{\alpha}{2}\sigma_y, \tag{22}$$

$$\langle i;j+1|H|i;j\rangle = -t\sigma_0 + i\frac{\alpha}{2}\sigma_x + i\frac{e\hbar}{2m^*}B_z\sigma_0, \tag{23}$$

where the hopping energy t is given by

$$t = \frac{\hbar^2}{2m^*a^2}. \tag{24}$$

Eq.(21) describes the particular energy on that tight-binding site. Terms in Eq. (22) describe the hoppings in positive x direction. Terms in Eq. (23) describe the hoppings in positive y direction. Any hopping in the opposite directions is simply the complex conjugate. The hopping energy between neighbouring sites is t which is a material specific parameter.

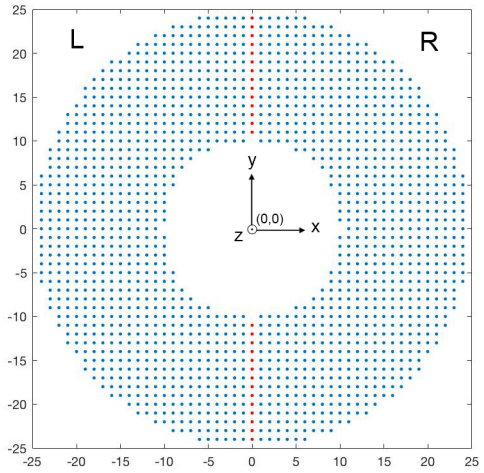

Figure 8: Schematic representation of the modeled system, each dot represents a tight binding site with red dots representing the barrier location separating the two dots (L) and (R) with the coordinate system orientation included in the center.

Each dot in Fig. 8 represents a tight binding site not to be confused with actual atoms. The distance between neighbouring sites is the lattice constant a. Each site is connected to adjacent sites by hopping energies. The central barrier

defining the double quantum dot system is visible as red marked dots.

It should be noted that a perfect ring has rotational symmetry meaning it remains unchanged when rotated by an arbitrary angle. As the model is discretized at a low resolution the ring is not perfect but has rough edges. This will directly influence the energy spectrum in a magnetic field and will be discussed in the appendix.

3.2 Angular Momentum

To evaluate the quality of the ring states it's illuminating to calculate the expectation value of the angular momentum operator

$$\langle \psi_i | \, L_z \, | \psi_i \rangle \,, \tag{25}$$

where ψ_i is the i'th eigenstate of the Hamiltonian. As the system is 2D there are no movement in the z-direction, this results in $L_x = L_y = 0$ and thus $\mathbf{L} = L_z$.

$$L_z^{can} = xp_y - yp_x = -i\hbar(x\frac{\partial}{\partial y} - y\frac{\partial}{\partial x}). \tag{26}$$

Here the canonical angular momentum is considered, not including the vector potential. In the Coulomb gauge, L_z^{can} is a conserved quantity (it commutes with the Hamiltonian). For a cylindrical symmetric system, it is also equal to the total L_z^{kin}, which is a conserved and gauge invariant quantity. Thus L_z^{can} is chosen to quantify how well the states correspond to a cylindrical symmetric system, which is a measure of the quality of the ring-like states. Calculating the matrix elements of L_z^{can} in the same position basis as the Hamiltonian results in

$$\langle i+1; j | \, L_z \, | i; j \rangle = \frac{i\hbar}{2a} y \sigma_0, \tag{27}$$

$$\langle i; j+1 | \, L_z \, | i; j \rangle = -\frac{i\hbar}{2a} x \sigma_0, \tag{28}$$

which add to the hopping terms. Again, hoppings in the opposite direction are given by complex conjugation. Ring states are necessary for observing a g-factor enhancement. Comparing L_z^{can} for different states can indicate good or poor ring formation.

3.3 Kwant

Kwant is an open-source python package for tight-binding simulations of quantum systems and is used throughout this project [3]. The package is designed to be user friendly and to have high performance using a combination of high and low level programming languages. Python is used to setup the system and to define the tight-binding Hamiltonian. The system is internally translated to a low level representation in C dealing with demanding numerical calculations and algorithms.

3.3.1 Building A System

Specifying the lattice and building the system can be done as follows

```
import kwant
lat = kwant.lattice.square(a)
sys = kwant.Builder()
```

where a is the lattice constant. Next up is specifying the shape and setting the onsite and hopping terms. The system considered is ring shaped and can be constructed by the following

```
sys[lat.shape(ring, (0, r1+1))] =
onsite

def ring(pos):
   (x, y) = pos
   rsq = x ** 2 + y ** 2
   return (r1 ** 2 < rsq < r2 ** 2)
```

where `lat.shape()` is a built-in function enabling one to pass a customized shape, here `ring` is a boolean function returning true for sites inside the ring where r1 and r2 is the inner and outer ring radius. `onsite` is a self-defined function that returns the onsite element from Eq (21). Passing functions to sites instead of fixed numbers makes the model more dynamic

as one does not need to rebuild the system when changing a parameter. Also, some terms require xy-position, passing the term as a function enables one to retrieve the position integer of the site as will be shown for `def hopy()` below.

Next the hopping terms are specified

```
sys[kwant.builder.HoppingKind((1,
0), lat, lat)] = hopx
sys[kwant.builder.HoppingKind((0,
1), lat, lat)] = hopy
```

where (1,0) and (0,1) are unit vectors that specify hoppings in x and y directions. Again the terms are passed as functions `hopx` and `hopy`. Next is an example of the y-hopping function stemming from Eq. (23) that can be passed to a site.

```
def hopy(site1, site2, B):
   (x, y) = site1.pos
   return -t * σ_0 - 1j * α * σ_x / 2
+ 1j * ħ / ( 2 * m* ) * B * x * σ_0
```

The hopping function requires two site arguments because it involves two sites. As the magnetic field is something one wish to vary this is passed as a parameter `B`. To get the position of a site one calls the `site1.pos` function which returns a tuple of the x and y coordinate. The last two lines of code returns the matrix element given by Eq. (23). The specific expression is dependent on the system geometry and terms included in the Hamiltonian. This concludes the building of the system.

3.3.2 Extracting and Diagonalizing the Hamiltonian

Extracting and diagonalizing the Hamiltonian is straightforward. Before any calculations are made the system needs to be finalized.

```
import scipy.linalg as la
sys = sys.finalized()
ham = sys.hamiltonian_submatrix()
evals, evecs = la.eigh(ham)
```

Here the `scipy.linalg` package was used to diagonalize the matrix. This gives the complete set of eigenvalues and vectors which often is excessive. To optimize performance the `scipy.sparse.linalg` packge can be used. Sparse matrix data structures are suitable for a tight-binding system as the matrix elements are mostly zeros. Moreover it enables the user to specify the desired number of eigenvalues and eigenvectors to be calculated. In this project, most often only the 10 lowest energy eigenstates are of interest and in dealing with matrix dimensions of up to 1000x1000, this option is crucial for code efficiency.

```
import scipy.sparse.linalg as sla
ham = sys.hamiltonian_submatrix(
params=dict(B=B), sparse=True)
evals = sla.eigsh(ham_mat.tocsc(),
k=10, sigma=0)
```

where k=10 specifies the number of eigenvalues and vectors to be calculated. The `params=dict(B=B)` command in the `hamiltonian_submatrix` function enables one to pass the magnetic field used in the onsite and hopping functions. As mentioned before this enables one to vary the magnetic field without rebuilding the system after it is finalized.

3.3.3 Modifying Potentials

In order to simulate attaching gate electrodes and detuning the quantum dot to create ring states as shown in Fig. 6, one can add a potential to the system. This is done by changing the energy of the system at desired locations by adding a potential function to the onsite terms which takes the site as a parameter. An example of how this is done is shown below

```
def potential(site, p):
   (x, y) = site.pos
   if x == 0:
      return V_barr
   if x < 0:
      return p
```

```
elif x > 0:
   return -p
```

This potential function adds a barrier `V_barr` for $x = 0$ in the system to separate the quantum dot into two dots left (L) and right (R), as illustrated in Fig. 8. It also symmetrically adds and subtracts the potential `p` to the left and right halves of the ring, yielding a potential asymmetry in the two half rings. This will be used for detuning of the system and will be discussed more in depth in Section 4.2.

3.4 Building the $\hat{L}$ Matrix Representation

To construct the matrix representation of the angular momentum operator in Eq. (26), Kwant can be used. By defining a separate system identical to the original model as done in Section 3.3.1, specifying the hopping terms according to Eq. (27 - 28) and retrieving the matrix by calling `hamiltonian_submatrix` function, in the same way as shown in Section 3.3.2. This is a neat way of obtaining the correct matrix which can be challenging to build by explicitly specifying the matrix elements. The expectation value in Eq. (25) is calculated by sandwiching the $\hat{L}$ matrix representation between the eigenvector of interest.

4 Results and Discussion

4.1 Ideal Ring

It's illustrating to start with the ideal ring case, that is without any barrier. The material parameters are shown in Table 1, excluding the barrier. Here the g-factor enhancement in a circular symmetric system with spin-orbit coupling can be observed by calculating the electron state energy evolution in **B** oriented along the z-direction [2].

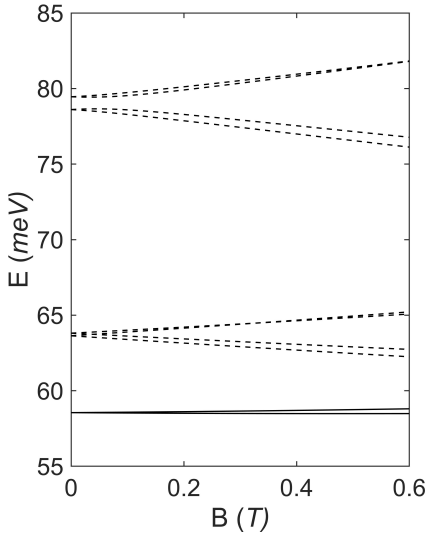

Figure 9: Energy levels in a uniform magnetic field along the nanowire z-direction for an ideal ring.

Including SOC splits the four fold degeneracy of states $l \neq 0$ (dashed lines in Fig. 9). The magnetic field **B** couples to the total magnetic moment, and as a result to the splitting of spin pairs [2]. In Fig 9 the $l = 0$ states (solid lines) have no orbital angular momentum and the states split by g^*_{spin}. In contrast, the higher angular momentum states states (dashed lines) which in a circular symmetric structure have non-zero orbital angular momentum (quantum ring states), have a significant splitting of the states due to the orbital contributions g^*_{orb} and thus experience g-factor enhancement, see section 1.1. The nonzero orbital angular momentum states, play a similar role in the g-factor enhancement in the double quantum dot which will be presented in the next Section 4.2.

4.2 Double Quantum Dot

The double quantum dot system is now considered. The material parameters used in the 2D tight-binding model are shown in Table 1.

Parameters	Value
Ring Outer Radius	25 nm
Ring Inner Radius	10 nm
Barrier Height	262 meV
Barrier Width	1 nm
Lattice constant a	1 nm
Rashba Spin-orbit constant α [1]	16 meV nm
g^*_{spin}	10
m_{InAs}	0.026 m_e
t	$1.4655 \cdot 10^3$ meV

Table 1. Model parameters for the DQD system

The system is detuned by shifting the energy levels of the two quantum dots relative to each other with the intention of aligning different orbitals. In practice the detuning is achieved by applying side gate voltages V_L and V_R as shown in Fig. 6. As explained in section 3.3.3, in the model this is achieved by adding and subtracting a symmetric potential to the onsite elements of the tight-binding Hamiltonian. Ring states in the double quantum dot system require alignment of even-odd orbitals, see section 1.1. The crossing of interest is between the second and third states of the (L) and (R) dot, the so called the (2,3) crossing. This is where the even-odd orbitals align and the formation of ring states are anticipated. The detuning is accompanied by calculating the angular momentum. There are 4 states involved in each of the (2,3) and (2,2) crossing and anti-crossing. By introducing a small magnetic field the angular momentum of the lowest energy state in each crossing is calculated.

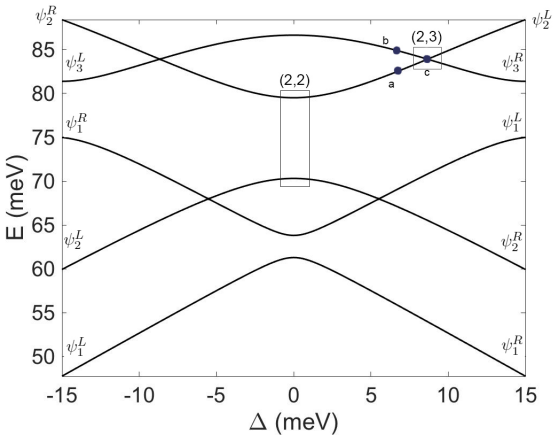

Figure 10: Energy levels in an electric field for an InAs double quantum dot at $\mathbf{B} = 0$. (2,3) crossing and (2,2) anti-crossing marked by squares. $|\langle \hat{L}_{2,3} \rangle| = 1.631\hbar$; $|\langle \hat{L}_{2,2} \rangle| = 0.0357\hbar$. Markings a,b and c is where the electron wave function is plotted below.

The detuning plot in Fig. 10 is in agreement with the findings of [1]. The states are labeled according to $\psi_n^{R/L}$ and represents the n'th eigenstate of the right (R) or left (L) dot. Δ is the detuning potential which is subtracted from the (R) dot and added to the (L) dot. Therefore ψ^R state energy decrease and ψ^L state energy increase for positive Δ detuning potential and the reverse for negative Δ. At $\Delta = 0$ the states are linear combinations of states in both dots with equal weights, thus its not possible to distinguish which state corresponds to which dot. Delocalized bonding and anti bonding orbitals are formed similar to that of molecules. For a perfect ring without barriers states would simply be eigenstates of the angular momentum operator and thus have integer eigenvalues $l_m = m\hbar$ at zero $\mathbf{B}$-field. Due to the barriers the states are 2-fold rather than 4-fold degenerate at $\Delta = 0$. Adding barriers destroyed the ring states at zero detuning, by adding a finite detuning the ring states are reformed at the (2,3) crossing, by realigning the energy levels of the two quantum dots. There is a tiny split due to spin-orbit interactions (SOI) in the (2,3) crossing, not visible in Fig. 10 but can be observed in Fig. 13. The (2,3) crossing between even and odd orbitals marked by a square in Fig. 10 is present at $\Delta = 8.7$ meV detuning potential. Plotting the probability density for the 2nd and 3rd state

close to the (2,3) crossing and at the crossing (a, b and c in Fig. 10) indicates the correct orbital combinations and the appearance of ring states, Fig. 11.

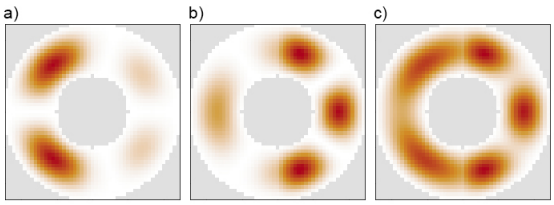

Figure 11: Magnitude square of the wave functions for a) ψ_2^L at $\Delta = 7$ meV, b) ψ_3^R at $\Delta = 7$ meV, c) one of the ring states in the (2,3) crossing at $\Delta = 8.7$ meV

In Fig. 11 a) and b) close to the (2,3) crossing, the (L) dot has an even orbital characterized as having 1 node in a quantum dot, whilst the (R) dot has an odd orbital (2 nodes) as expected. This confirms that the (2,3) crossing is in fact combinations of even and odd states similar to the (L) and (R) dot in the even-odd state schematic illustration in Fig. 4. In Fig. 11 c) at the (2,3) crossing the 2nd and 3rd states becomes two ring states split by spin orbit coupling. The ring states are characterized by vanishing nodes and having a more uniform charge distribution in both QDs. Ín a perfect ring the wave functions would be completely uniform. The angular momentum for the lowest energy state at this configuration is significant, $|\langle \hat{L}_{2,3} \rangle| = 1.631\hbar$ also indicating the formation of ring states. The angular momentum of the other ring state involved in the (2,3) crossing is similar. On the other hand the angular momentum of the (2,2) anti-crossing at $\Delta = 0$ signifies poor ring formation, as $|\langle \hat{L}_{2,2} \rangle| = 0.0357\hbar$. It confirms that even-even (and similarly odd-odd) orbital combinations are poor candidates for ring formations as mentioned in section 1.1.

To observe the g-factor enhancement the state energies are evaluated under the influence of a magnetic field applied along the z-direction as done for the ideal ring in Fig. 9 but at a finite detuning $\Delta = 8.7$ meV required for the (2,3) crossing.

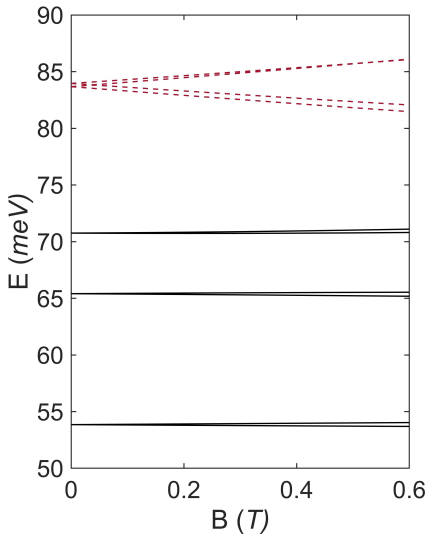

Figure 12: Energy levels in a uniform magnetic field along the nanowire z-direction for an InAs double quantum dot with $\Delta = 8.7$ meV detuning potential.

In Fig. 12 (b) the detuning potential $\Delta = 8.7$ meV is fixed whilst sweeping the magnetic field from 0 to 0.6 T. In this way the response of the energy levels to a finite magnetic field is observed. There is an increased splitting of the states involved in the (2,3) crossing (red dashed) compared to the lowest states (solid lines) and this is due to the orbital contributions to the g-factor of aligned even and odd orbitals and thus formation of ring states. This is similar to the splitting of the higher angular momentum states (dashed lines) in the ideal ring in Fig. 9. To quantify the results the states involved in the (2,3) crossing are plotted separately in Fig. 13.

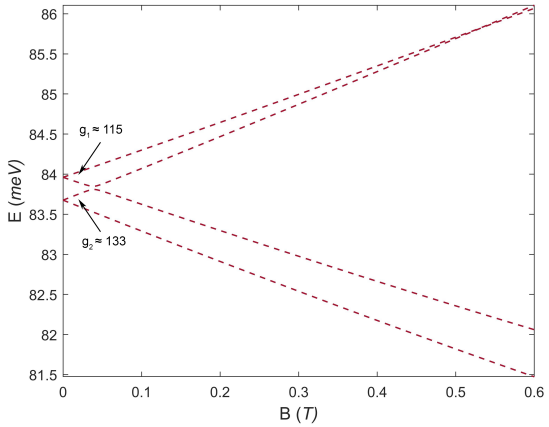

Figure 13: The energies of the states involved in the (2,3) crossing in a uniform magnetic field with an estimate of the effective g-factors.

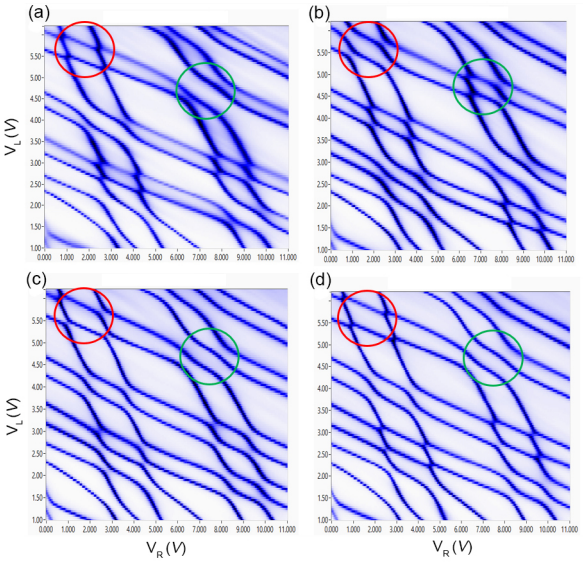

Figure 14: Experimental results on AB oscillations in DQDs. (a) 0 T (b) 1 T (c) 2 T (d) 2.5 T corresponding to 1 h/e. Figure taken from [19].

The effective g-factor represents the splitting between the two spin pairs in the presence of a magnetic field. In this case, this is only relevant for small $\mathbf{B}$ as the states anti-cross around $\mathbf{B}$ = 0.025 T due to SOI. The effective g-factor is calculated by extracting g^* from the split in energy between the two spin pairs given by $g^*\mu_B B_z$ at 0.01 T. The effective g-factors at low field $g_1 \approx 115$ and $g_2 \approx 133$ are significantly larger than the bulk g-factor for InAs ($g^*_{spin} = 10$) and agrees with previous findings [1] [2] and is attributed to the coupling of the non-zero orbital angular momentum states to the external magnetic field and thus orbital contributions g^*_{orb} to the effective g-factor g^*.

To further model recent and unpublished experimental findings of AB oscillations (see section 1.1.1) in quantum rings [19] their result are presented here. Their experimental system is essentially what is modeled in this thesis with some slight differences. In summary a $\Theta = 80$ nm diamater (compared to 50 nm in the model) InAs NW with a strongly depth confined DQD. By adjusting side gates at different $\mathbf{B}$ parallel to the NW, the AB oscillations can be observed and their result is shown in Fig 14.

The detuning in experiments is achieved by adjusting the left (V_L) and right (V_R) side gate potentials. In Fig. 14 going from (a) $\mathbf{B}$ = 0 T to (b) $\mathbf{B}$ = 1 T the states in red and green circles, corresponding to (2,3) crossing and (2,2) anti-crossing respectively are disrupted as the states in the red circle are starting to split while the green circle states start to cross. From (b) $\mathbf{B}$ = 1 T to (c) $\mathbf{B}$ = 2 T the states start to return to their original configuration and at (d) at $\mathbf{B}$ = 2.5 T corresponding to 1 h/e the states reform similar to that of (a). To observe this in the model the detuning plot in Fig. 10 is reproduced for key $\mathbf{B}$-field values corresponding to the ring being penetrated by the flux $\phi = \frac{1}{4}, \frac{1}{2}, \frac{3}{4}, 1$ h/e. The area which corresponds to 1 flux quantum is obtained from finding the required $\mathbf{B}$-field for completing one period of the AB oscillation which was $\mathbf{B}$ = 4.5 T. This corresponds to a radius which is half way in between the inner and outer ring radius. This is reasonable since this is where the electron density should be centered. In Fig. 14 one period correspond to 2.5 T, however the system is larger than the one used in this thesis. The detuning plots are also accompanied by calculating the angular momentum expectation value again for the lowest energy state involved

in the (2,3) and (2,2) crossings.

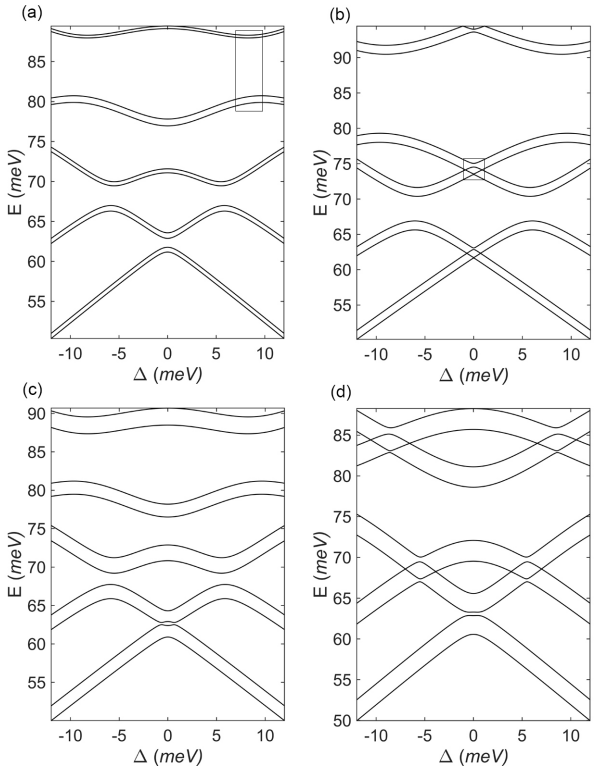

Figure 15: Energy levels for **B**-field values corresponding to characteristic flux values with the respective angular momentum expectation value for the (2,3) and (2,2) anti-crossings. (a) $\mathbf{B} = 1.125$ T; $\phi = \frac{1}{4}$ h/e. $|\langle \hat{L}_{2,3} \rangle| = 1.402\hbar$; $|\langle \hat{L}_{2,2} \rangle| = 0.584\hbar$, (2,3) anti-crossing marked by square. (b) $\mathbf{B} = 2.25$ T; $\phi = \frac{1}{2}$ h/e. $|\langle \hat{L}_{2,3} \rangle| = 0.527\hbar$; $|\langle \hat{L}_{2,2} \rangle| = 1.002\hbar$, (2,2) crossing makred by square. (c) $\mathbf{B} = 3.375$ T ; $\phi = \frac{3}{2}$ h/e. $|\langle \hat{L}_{2,3} \rangle| = 1.476\hbar$; $|\langle \hat{L}_{2,2} \rangle| = 0.654\hbar$. (d) $\mathbf{B} = 4.5$ T ; $\phi = 1$ h/e. $|\langle \hat{L}_{2,3} \rangle| = 1.667\hbar$; $|\langle \hat{L}_{2,2} \rangle| = 0.285\hbar$

In Fig. 15 (a) at $\mathbf{B} = 1.125$ corresponding to $\phi = \frac{1}{4}$ h/e the states involved in the (2,3) crossing marked by square start to split due to the incorporation of the vector potential into the Hamiltonian similar to previous plots (Fig. 12 - Fig. 13) and thus as a result of the AB effect, see section 1.1.1. Like before the individual energy levels also start to split due to the Zeeman effect. The angular momentum for the (2,3) crossing decreases from $1.631\hbar$ in Fig. 10 to $1.402\hbar$ indicating the magnetic field is disrupting the ring states and is reflected in a decreasing angular momentum. In Fig. 15 (b) at $\phi = \frac{1}{2}$ h/e the even-odd parity requirement for ring states is reversed. In (b), the anti-crossing of the (2,3) states (marked by square in (a)) is maximal which is reflected in the lowest $|\langle \hat{L}_{2,3} \rangle|$ of $0.527\hbar$. This is also where the angular momentum of the (2,2) crossing obtains its largest value of $|\langle \hat{L}_{2,2} \rangle| = 1.002\hbar$. At $\phi = \frac{1}{2}$ h/e the even-even and odd-odd states form ring states instead of the even-odd states as another minus sign is introduced in one of the tunneling couplings, discussed in section 1.1. The connection between the ring states and the sign of the tunnel coupling will be explained in detail below. Continuing to Fig. 15 (d) at **B** = 4.5 T corresponding to $\phi = 1$ h/e the (2,3) crossing is realigned revealed by crossing of the (2,3) states comparable with Fig. (10) apart from the now prominent Zeeman splitting. The fact that the states cross at this flux magnitude indicates the correct flux induced phase shifts in the Hamiltonian and concludes one period 2π of the AB oscillation. Meaning threading 1 h/e through the ring leaves the electrons in the same phase as for zero field $e^{i\phi_0/2} = e^{i(\phi_0+2\pi)/2}$, see section 1.1.1. The $|\langle \hat{L}_{2,3} \rangle| = 1.667\hbar$ for this state is comparable to the angular momentum at zero **B**-field in Fig. 10, indicating the ring states are in fact reformed.

The difference in energy splittings between (2,2) and (2,3) crossings was explained in [1] by the use of degenerate perturbation theory in a simpler 1D chain. Here we want to make use of this model and include the magnetic field to gain further insight into the above results. The unperturbed system was regarded as two separated (L) and (R) 1D quantum wells described by sinusoidal wave functions which in a tight-binding setting read

$$|\psi^0_{L,n}\rangle = \sum_{\sigma,j=1}^{N/2} a_{L,n,j,\sigma} |\phi^0_{L,j,n}\rangle \tag{29}$$

$$|\psi^0_{R,n}\rangle = \sum_{\sigma,j=\frac{N}{2}+1}^{N} a_{L,n,j,\sigma} |\phi^0_{R,j,n}\rangle \tag{30}$$

where $a_{L/R,n,j,\sigma}|\phi^0_{L/R,j,n}\rangle$ are the (L) and (R) wavefunction and coefficient at site j for spin $\sigma = \uparrow, \downarrow$ for the n'th state in the QD. The (L)

dot consists of sites 1 to N/2, while the (R) dot consists of sites N/2+1 to N. The particle in a box wave functions obey

$$\begin{aligned} a_{L,n,1,\sigma} = a_{L,n,N/2,\sigma} = a;\ for\, n\, odd, \\ a_{L,n,1,\sigma} = -a_{L,n,N/2,\sigma} = a;\ for\, n\, even, \\ a_{R,n,\frac{N}{2}+1,\sigma} = a_{R,n,N,\sigma} = a;\ for\, n\, odd, \\ a_{R,n,\frac{N}{2}+1,\sigma} = -a_{R,n,N,\sigma} = a;\ for\, n\, even, \end{aligned} \tag{31}$$

where a can be chosen positive or negative. When the levels in Eq (29 - 30) align they form a degenerate subspace. In [1] the perturbation is regarded in the form of coupling between sites at the two tunneling connection points 1,N and N/2, N/2+1. To reveal how the magnetic field affects the energy corrections in the perturbation from [1], and thus if it is in agreement with the results from the model above, the flux induced phase shift $e^{i\frac{\phi}{2}}$ is incorporated into the perturbation below, considering only one spin

$$\delta H = -t(c^{\dagger}_{\frac{N}{2},\uparrow}c_{\frac{N}{2},\uparrow}e^{i\phi/2} + c^{\dagger}_{N,\uparrow}c_{1,\uparrow}e^{-i\phi/2} + H.C.)$$

$$+t_{soc}(-ic^{\dagger}_{\frac{N}{2},\uparrow}c_{\frac{N}{2},\uparrow}e^{i\phi/2} - ic^{\dagger}_{N,\uparrow}c_{1,\uparrow}e^{-i\phi/2} + H.C.). \tag{32}$$

where $c^{\dagger}_{j,\sigma}$ ($c_{j,\sigma}$) creates (annihilates) an electron with spin $=\uparrow,\downarrow$ at site j. Sandwiching Eq.(32) between (29 - 30) yields the matrix representation of the perturbation in the degenerate subspace. First the case of $\mathbf{B} = 0$ corresponding to $\phi = 0$ is studied where the $|\psi^0_{L,2}\rangle, |\psi^0_{R,2}\rangle$ are aligned. Diagonalization of the perturbation matrix in the degenerate subsapce yields that the (2,2) is split by t, where t is the hopping energy between neighbouring sites. At $|\psi^0_{L,2}\rangle, |\psi^0_{R,3}\rangle$ orbital alignment the states are split by t_{soc}, where $t_{soc} = \alpha/2a$. The fact that t is many times larger than t_{soc} results in a large difference in the (2,2) and (2,3) energy splitting, as is observed in Fig. 10. Performing the same calculation for $\phi = \pi$ corresponding to flux equal to $\frac{1}{2}\ h/e$ reveals that the case is reversed. Now the (2,2) states split by t_{soc} and (2,3) are split by t. This is in agreement with the AB oscillations in Fig. 15 (b).

5 Conclusion and Outlook

In this report we have studied a double quantum dot system consisting of a ring shaped 2D tight-binding lattice with the two quantum dots separated by barriers. The system includes en extension of previous theory in [1] to a more complex and realistic model which in turn can yield a more accurate and insightful picture of experimental results. A g-factor enhancement could be straightforwardly observed in agreement with previous experimental findings and theoretical models [1] [2], thus proving the underlying physics is intact. There are quantitative indications of the formation of ring states as an explanation for the g-factor enhancement. These include significant angular momentum of the involved states when the 2nd orbital on one dot aligns with the 3rd orbital on the other dot, the so called (2,3) crossing. Also, the states involved in the (2,3) crossing exhibit significant splitting in a magnetic field indicating orbital contributions from ring states, similar to that of the ideal ring and in agreement with previous findings of ring states in similar systems [2].

Moreover AB oscillations are observed in the system when a significant magnetic field is applied such that the ring is penetrated by a large flux. The oscillations demonstrate how the (2,3) crossing undergoes transformation from crossing to anti-crossing going from $\phi = 0$ to $\frac{1}{2}\ h/e$ and the angular momentum of the (2,3) crossing obtains its minimum. In contrast, the (2,2) anti-crossing becomes a crossing with states of significant angular momentum at $\phi = \frac{1}{2}\ h/e$ indicating formation of ring states. Thus the orbital parity requirements for good rings are reversed. These results are supported by a degenerate perturbation theory analysis which predicts as small splitting for the (2,3) crossing and a large splitting of the (2,2) anti-crossing at $\phi = 0\ h/e$, while the situation is reversed at $\phi = \frac{1}{2}\ h/e$.

An illuminating extension of the model could include different ring shapes such as hexagonal or square rings and in a consistent way follow the impact on the result, giving more insight into the symmetry dependence of the AB oscillations [16].

To observe the findings of highly anisotropic effective g-factors in [1] the magnetic field could be applied in different orientations. This would be straight forward to include in the model. Another extension of the model would be considering the 3D system. Because of the efficiency of the calculations this would most likely be numerically possible to implement in Kwant. In practice this could be achieved by stacking the current 2D model in layers with hoppings connecting them. This could possibly yield an even better picture of the experimental system.

In general, Kwant which is focused on transport calculations, has been a solid tight-binding package even for stationary problems. It's fairly easy to adapt and get started with and has a variety of customization possibilities and an extensive documentation. It could have been useful to know more about how the system is internally translated to enable further modification and make visualization of the system using other plotting software more accessible. The calculation efficiency is decent when complementing with sparse matrices and an estimated time frame for diagnolaizing the Hamiltonian presented in this thesis are in the regime of seconds.

The ability to control the ring states from good to bad and back again by tuning the magnetic field possibly enables interesting applications in controlling spin properties, for example in spin qubits. Another topic is the coupling of the double quantum dot system to a superconductor in order to study the emergence of Majorana bound states, which has possible applications in topological quantum computation. As magnetic field suppresses superconductivity but is required to induce a topological phase transition, it's desirable to have large g-factors. Therefore the ability to tune the g-factor over a wide range in materials with strong SOC (InAs, InSb) could be of great value in the years to come [2].

6 APPENDIX A

6.1 AB Symmetry Breaking

The presence of the Aharonov-Bohm effect is independent of the symmetry of the system as long as the electron travels in a closed loop around the magnetic field. However the symmetry of the system does affect the energy spectrum. In an ideal ring there is rotational symmetry C_∞, meaning the system is symmetric under rotations by an arbitrary angle. This symmetry group has an infinite amount of irreducible representations and leads to an infinite amount of energy states with different symmetry [16]. Together with the effect of magnetic flux on the electron state energy, the AB effect is reflected in continuous crossings of energy levels as a function of magnetic field, Fig. 16 (a).

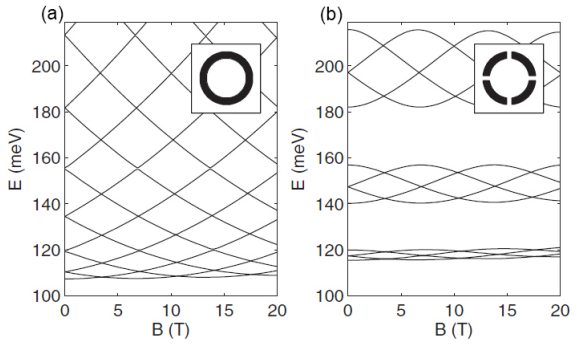

Figure 16: Electron energies as a function of magnetic field strength. (a) Circular symmetric system C_∞ (b) 4-fold symmetric system C_4. Figure taken from [20].

Introducing horizontal and vertical barriers on the C_∞ ring in Fig. 16 enforces 4-fold symmetry C_4, where the system is symmetric under rotations by an angle $\frac{\pi}{2}$. The degeneracy of states in C_∞ are broken in the C_4 system. The result is anti-crossing regions repeating for electron states $m = \pm 2, \pm 4, \pm 6...$ and orbital states are grouped in 4 separated by bandgaps [20], Fig. 16 (b). In general, a system with finite confinement potential n (C_n) electron states are grouped in numbers of n separated by anti-crossing regions or bandgaps.

Ideal rotational symmetry C_∞ does not hold for ring states in the discretized model. In Fig. 17 (a) there are no obvious indications of symmetry breaking however the effect becomes more evident when increasing the inner radius corresponding to a thinner ring system.

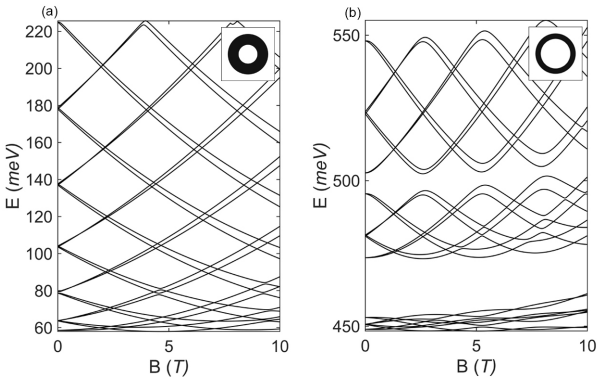

Figure 17: Electron energies as a function of **B**-field strength. (a) Inner ring radius = 10 nm showing a behaviour close to that of a perfect ring (C_∞ symmetry). (b) Inner ring radius = 20 nm showing a behaviour closer to that of a C_4 symmetric system.

Fig. 17 (a) shows the state energy evolution in a **B**-field for parameters used in the main text. In (b) the inner radius is set to 20 nm corresponding to a thinner ring. The result is a grouping of energy states in $n = 4$ similar to Fig. 16 when moving from C_∞ to C_4. This is directly caused by the discretization. A discretized ring at this low resolution leads to rough edges where the site pattern of the edges seems to be symmetric under rotations of $\frac{\pi}{2}$, corresponding to C_4. Having a thicker ring seems to reduce the effect of state grouping and the system behaves more like C_∞, due to the electron wave function being less affected by the edges.

References

[1] H. Potts, I.-J. Chen, A. Tsintzis, M. Nilsson, S. Lehmann, K. A. Dick, M. Leijnse, and C. Thelander, "Electrical control of spins and giant g-factors in ring-like coupled quantum dots.", *Nature Communications*, vol. 10, p. 5740, 2019.

[2] G. W. Winkler, D. Varjas, R. Skolasinski, A. A. Soluyanov, M. Troyer, and M. Wimmer, "Orbital contributions to the electron g-factor in semiconductor nanowires.", *Phys. Rev. Lett*, vol. 119, p. 037 701, 2017.

[3] C. W. Groth, M. Wimmer, A. R. Akhmerov, and X. Waintal, "Kwant: A software package for quantum transport.", *New J. Phys*, vol. 16, p. 063 065, 2013.

[4] "International roadmap for devices and systems, executive summary", IEEE, Institute of Electrical and Electronics Engineers, Tech. Rep., 2020.

[5] M. A. Nielsen and I. L. Chuang, *Quantum Computation and Quantum Information: 10th Anniversary Edition*, 10th. USA: Cambridge University Press, 2011, ISBN: 1107002176.

[6] M. Nilsson, "Charge and spin transport in parallel-coupled quantum dots in nanowires.", PhD thesis, Lund University, 2018.

[7] A. Shields, "Semiconductor quantum light sources", *Nature Photonics*, vol. 1, p. 215, 2007.

[8] T.-H. Kim, K.-S. Cho, E. K. Lee, S. J. Lee, J. Chae, J. W. Kim, D. H. Kim, J.-Y. Kwon, G. Amaratunga, S. Y. Lee, B. L. Choi, Y. Kuk, J. M. Kim, and K. Kim, "Semiconductor quantum light sources", *Nature Photonics*, vol. 5, p. 176, 2011.

[9] D. Loss and D. P. DiVincenzo, "Quantum computation with quantum dots", *Phys. Rev. A*, vol. 57, pp. 120–126, 1998.

[10] T. Biktagirov and U. Gerstmann, "Spin-orbit driven electrical manipulation of the zero-field splitting in high-spin centers in solids", *Phys. Rev. Research*, vol. 2, p. 023 071, 2 2020.

[11] F. Glas, "Critical dimensions for the plastic relaxation of strained axial heterostructures in free-standing nanowires", *Phys. Rev*, vol. 74, p. 121 302, 2006.

[12] J. Johansson and K. A. Dick, "Recent advances in semiconductor nanowire heterostructures", *CrystEngComm*, vol. 13, p. 7175, 2011.

[13] J. Salfi, S. Roddaro, D. Ercolani, L. Sorba, I. Savelyev, M. Blumin, H. E. Ruda, and F. Beltram, "Electronic properties of quantum dot systems realized in semiconductor nanowires", *Semicond. Sci. Technol*, vol. 25, p. 024 007, 2010.

[14] F. Koppens, C. Buizert, K. Tielrooij, *et al.*, "Driven coherent oscillations of a single electron spin in a quantum dot", *Nature*, vol. 442, pp. 766–771, 2006.

[15] Y. Aharonov and D. Bohm, "Significance of electromagnetic potentials in the quantum theory", *Phys. Rev.*, vol. 115, pp. 485–491, 3 1959.

[16] A. Clavería Díaz, "A pedagogical approach to the aharonov bohm effect," Universitat Jaume I, 2018.

[17] R. A. Webb, S. Washburn, C. P. Umbach, and R. B. Laibowitz, "Observation of $\frac{h}{e}$ aharonov-bohm oscillations in normal-metal rings", *Phys. Rev. Lett.*, vol. 54, pp. 2696–2699, 25 1985.

[18] R. Winkler, "Spin–orbit coupling effects in two-dimensional electron and hole systems", *Springer Berlin Heidelberg*, 2003.

[19] R. Debbarma, H. Potts, Sebastian, K. Dick Thelander, C. Thelander, A. Tsintzis, and M. Leijnse, "Symmetry and parity effects on the aharonov-bohm phase of a quantum ring", *Lund University, Unpublished draft*,

[20] P. J, R. F, and C. J I, "Electron states in quantum rings with structural distortions under axial or in-plane magnetic fields.", *Nanotechnology*, vol. 18, no. 37, p. 375 402, 2007, ISSN: 09574484.